Three-dimensional confocal thermal imaging using anti-Stokes luminescence

A. V. Kachynski, A. N. Kuzmin, H. E. Pudavar, and P. N. Prasad[a)]
The Institute for Lasers, Photonics, and Biophotonics, Department of Chemistry, SUNY at Buffalo, Buffalo, New York 14260-3000

(Received 19 November 2004; accepted 25 May 2005; published online 6 July 2005)

High-resolution thermal images of dye-stained live cells are obtained using confocal anti-Stokes luminescence on a confocal laser scanning microscope. Stokes and anti-Stokes fluorescence signal ratio imaging, using dual laser excitation with a fast alternate line scan, is used to monitor dynamical temperature changes at submicrometer resolution. Temperature mapping of a dye-doped polymer film with local heating is shown as an example. Three-dimensional mapping of local temperature changes in living cells induced by an external laser as the heating source, is obtained with temperature resolution better than 0.5 K. © *2005 American Institute of Physics*.
[DOI: 10.1063/1.1993761]

In the last 50 years, there have been a few reports of temperature monitoring using noninfrared, noninvasive techniques which utilize changes in the emission spectra of doped dyes.[1–6] One example of such techniques is the anti-Stokes luminescence (ASL) phenomenon[7–10] which was intensively studying in 1970s.[8] However, there has been no report of confocal or other optical imaging method to provide three-dimensional (3D) mapping of temperature with high spatial resolution. Here we report an approach to high resolution, 3D thermal imaging utilizing the phenomenon of ASL, together with dual laser excitation confocal imaging.

Conventional fluorescence, or Stokes emission, occurs from the optical excitation of molecules in the zero point vibrational level of the ground electronic state to the first excited electronic state and a subsequent radiative decay to the ground state. In case of ASL, the optical excitation occurs from thermally excited vibrational-rotational energy states of the ground state. Since the population of the upper vibrational levels of the ground state is temperature dependent (based on Boltzman distribution), the ASL intensity is extremely temperature dependant[10] (exponential dependence) as represented by the following equation:

$$I(T) \sim A \exp(-\Delta E/kT), \tag{1}$$

where $I(T)$ is the ASL intensity of the dye solution at temperature T, A is a proportionality coefficient, k is the Boltzmann constant, and ΔE is the activation energy to the thermally populated level. A detailed physical description and applications of the ASL for measuring local temperature variations can be found elsewhere.[7–10] A large variety of fluorescent dyes and quantum dots exhibit the ASL phenomena when excited using appropriate excitation sources.

In this letter, we demonstrate the usage of the ASL phenomenon for high-resolution three-dimensional thermal imaging. We used a commercial dye, Rhodamine 640 (also known as Rhodamine 101, from Exciton Inc.). It can be excited at 488 nm (argon laser line) for conventional fluorescence while it can also be excited at 632.8 nm (He–Ne laser line) for anti-Stokes luminescence.[9,10] Figure 1(a) presents the ASL spectra of a Rhodamine 640 (Rh640) solution with 632.8 nm excitation. To measure the temperature dependence of the ASL intensity, we used an inverted microscope (Nikon) equipped with He–Ne and Nd: yttrium–aluminum–garnet (YAG) ($\lambda = 1064$ nm) lasers. The coincident laser beams were introduced into the microscope by the optical system that allowed the beams to be focused to a diffraction limited spot ($1/e^2$ spot diameter <1 μm). A 632.8 nm line from the He–Ne laser was used as the ASL excitation source. A continuous-wave high intensity Nd:YAG laser provided direct two-photon excitation of the Rh640 dye solution. The intensity of the two-photon excited emission was measured as a reference to normalize the ASL intensity. This compensates for the influence of the concentration fluctuation in the dye solution, occurring during the measurement. Curve 2 of

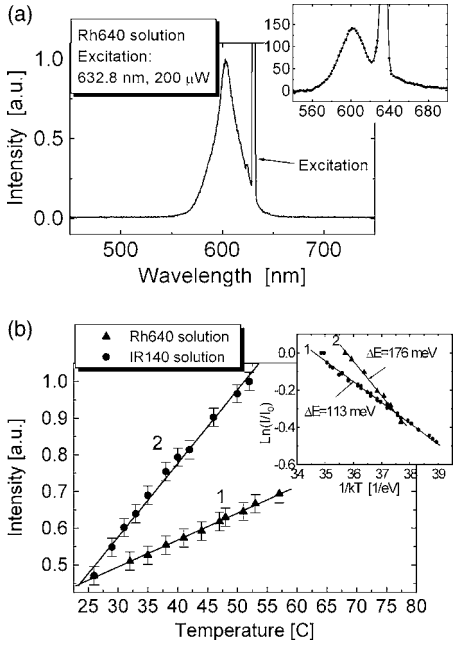

FIG. 1. (a) ASL spectrum of Rhodamine 640 solution and Rhodamine 640 dye encapsulated in 35 nm silica shells (inset); (b) temperature dependence of ASL for Rh640 solution (●) (excitation—He–Ne laser, $\lambda = 633$ nm) and IR-140 solution (▲) (excitation—Nd:YAG laser, $\lambda = 1064$ nm). The activation energy estimated for each dye is shown in the figure inset and this calibration is used for temperature mapping under confocal microscope.

a)Electronic mail: pnprasad@acsu.buffalo.edu

Fig. 1(b), shows the temperature dependence of the normalized anti-Stokes luminescence intensity of the Rh640 solution. For estimation of the activation energy ΔE using Eq. (1), the normalized ASL intensity is plotted on a log scale against $1/kT$, as shown by curve 2 of Fig. 1(b) inset. The ΔE value provided a calibration plot that is used for temperature estimation inside unknown samples containing the same Rh640 dye. The inset in Fig. 1(a) shows the ASL spectra of the same dye, when encapsulated[11] in 35 nm size silica nanoparticles. We have also tested another commercial dye IR-140 (Exciton Inc.), as well as InP quantum dots (not shown) for ASL.

By choosing a proper combination of the dye and the excitation wavelength, it is possible to enhance the temperature sensitivity of ASL. For example the dye IR-140, under 1064 nm excitation [curve 2 in Fig. 1(b)], shows a significantly higher sensitivity to temperature than Rh640 under 632.8 nm excitation [Fig. 1(b), curve 1]. We estimate the temperature measurement accuracy of our system to be 0.5 K based on our calibration parameters and sensitivity of the detection system. Using the same dye/laser combination, but with better detection system this accuracy can be less than 0.2 K, as reported by Clark *et al.*[10]

We have adapted this temperature measurement method for high-resolution three-dimensional imaging. A commercial confocal laser scanning microscope was used to measure the vertical (Z) set of ASL intensity distributions in several horizontal (XY) planes of a sample. While imaging real samples, the ASL intensity obtained from different (spaced) sample points depends on both the local temperature and the local dye concentration. Since the dye distribution inside a sample may not be uniform, we have to separate these two factors to obtain the true temperature map of the samples. Consequently, we used conventional Stokes fluorescence images to map the dye distribution inside the sample, and utilized these data to normalize the ASL intensity. Thus, to get a 3D thermal image, we measured the luminescence intensity distribution $I(X,Y,Z)$ of the sample in ASL and in Stokes luminescence modes, using a confocal microscope. Then the ASL intensity at each point was normalized with the corresponding Stokes luminescence intensity using custom software. Using the previously obtained calibration data, i.e., ΔE and Eq. (1), the corrected ASL intensity distribution $I(X,Y,Z)$ was converted to a temperature distribution $T(X,Y,Z)$.

A commercial confocal microscope (Bio-Rad MRC-1024), equipped with He–Ne and Ar ion lasers as excitation sources, was used for imaging. Samples were prepared either by direct incorporation of the dye, Rh640, into them or by coating a Rh640 doped polymer film on to them. These samples were imaged first using 488 nm (10 μW at the image plane) excitation (Stokes emission) to map the dye concentration, and subsequently imaged using 632.8 nm (400 μW at the image plane) long-wavelength edge excitation (anti-Stokes emission). A holographic Super-Notch filter (optical density, OD$>$4) that cutoff the scattered 632.8 nm light, and a long pass filter (OG515) that cutoff 488 nm excitation, were used in front of the detector. The detector gain and other imaging parameters were adjusted to avoid detector saturation at higher sample temperatures. For each point (pixel) in the raster-scanned image, the anti-Stokes intensity emission was normalized with that of the Stokes emission (so-called ratio image) and the temperature was calculated for each point in the image plane, using the calibration plot [curve 2 of Fig. 1(b)]. An inhomogeneous temperature distribution in the sample produces an inhomogeneous ASL intensity (normalized) distribution; thus each pixel in the image will exhibit an intensity, corresponding to the temperature dependence of ASL intensity shown in Fig. 1(b).

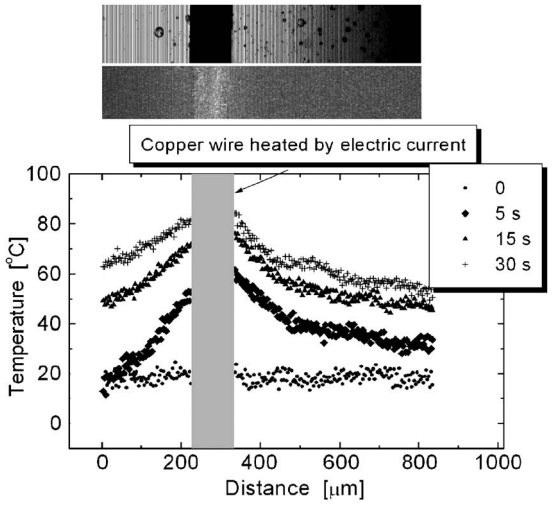

FIG. 2. Thermal images and temperature distribution of a 120 μm poly(methylmethacrylate) film containing Rh640. A copper wire with diameter $\sim$120 μm is incorporated in the sample for heating. (a) Transmission image showing the metal wire and the polymer film (wire is seen as a dark vertical stripe). (b) Thermal image of the sample, when it is heated by electric current $\sim$2 A passing through the copper wire (30 s after current was switched on). (c) Average horizontal Y profiles of temperatures (dots) extracted from the center of thermal images, obtained before switching of the current (0 s) and after 5, 15, and 30 s.

For imaging dynamic events, any time shift between obtaining Stokes and anti-Stokes images is not acceptable as it can be detrimental to the accuracy of the temperature estimate. This is particularly crucial in the case of live cell imaging. To circumvent this problem we modified our confocal microscope to obtain fast ratio imaging. In this method, two laser beams (one to generate Stokes emission and the other to generate ASL) are passed through two individual shutters, based on an acousto-optic modulator, then combined using a beam splitter, and coupled into the confocal microscope. Lasers 1 and 2 are turned on and off using line synchronization signals available from the microscope controller, so that the raster scanned image contains alternate lines with different excitations. The image is acquired in a high-resolution mode, so that the spacing ($<$0.3 μm) between the two lines in the image is smaller than the optical resolution of the system. Once the image is acquired, custom software splits the image into two images for the different excitation wavelengths. This method of ratio imaging allows almost simultaneous acquisition of two images with two different laser excitations (temporal separation between two laser scans can be as small as 500 μs). Some thermal images obtained using this method, are shown in Figs. 2 and 3. In the first example, a Rh640-doped polymer film (polymethylmethacrylate) containing a metal wire, inserted for local electrical heating was imaged [Figs. 2(a) and 2(b)] under the confocal microscope. Figure 2(c) shows the radial temperature distribution at different time points during heating, when an electric current of 2 A was passing through the wire. A high-resolution temperature mapping technique can also be used in bio-imaging. Though most of the biologically significant parameters such

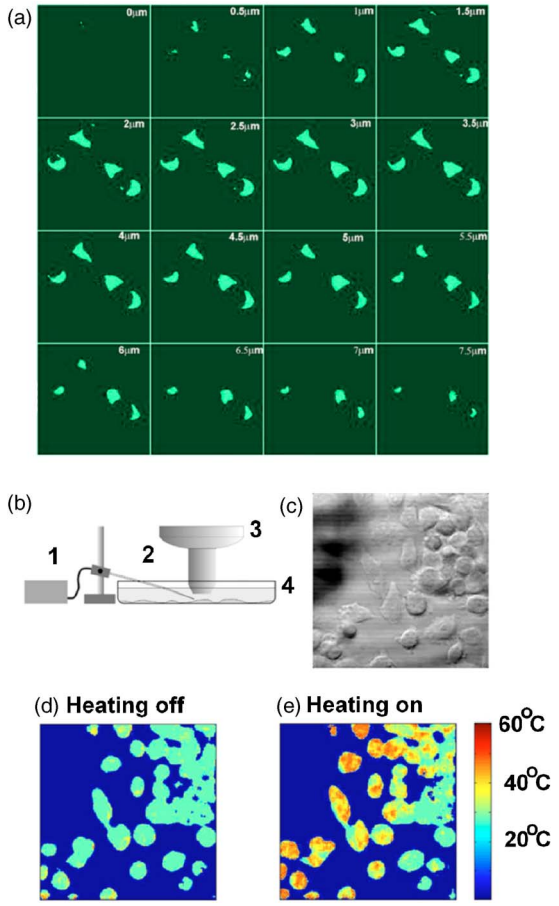

FIG. 3. (a) (Color online). A series of thermal images at different depths of KB cells stained with Rh640. They were acquired at 0.5 μm steps. (b) Schematic diagram showing the experimental setup used for heating live cells under the microscope objective (3). (c) Shows the transmission image of the cells. The shadow on the left top corner is due to the optical fiber (2), used for delivering the 1.9μm laser (1) radiation to locally heat the Rhodamine 640 stained cells in a Petri dish (4). The color-coded images shown in (d) and (e) are the thermal images obtained when the heating laser is turned on and off. The colorbar on the right side shows the color-coded temperature scale (°C) used in the images.

as *p*H,[12] electrical potential,[13] or ion concentration[12,14] have been monitored using confocal microscopy with high spatial resolution in three dimensions, 3D mapping of the temperature in tissues or cells at high spatial resolution has never been achieved. We applied our thermal imaging approach to KB cells (a human carcinoma cell line) stained with the dye Rh640. In this experiment, 50 μl of a 10 μM Rh640 solution in a dimethylsulfoxide/water mixture was added directly to the 35 mm cell culture Petri dish, and incubated for 30 min. After incubation, cells were washed with the culture media to remove all the free dye, and then imaged under the confocal microscope using a 60× water immersion objective.

The results of monitoring the three-dimensional temperature distribution inside the living individual KB cells, are shown in Fig. 3(a). The series of images were acquired at 0.5 μm steps along the *Z* (axial) direction; we did not find much variation in temperature (~37 °C) across the cell. This is not surprising, since healthy live cells are well known to be very good in controlling temperature inside them. But this might not be the case in the event of diseases or laser therapy, ultrasonic treatment, or under the action of other external agents such as photodynamic therapy drugs[15,16] or during chemotherapy.[17]

To introduce a temperature gradient into the biosample, we locally heated the cells by using an infrared radiation from a diode-pumped cw $Tm^{3+}:KGd(WO_4)_2$ laser (λ =1.9 μm), and monitored the temperature changes in a sample during the heating-cooling cycle. For this purpose the 1.9 μm laser beam was delivered into a section of the imaging area, using a tapered optical fiber. Figure 3(b) shows an schematic diagram of the experimental setup; Fig. 3(c) shows the transmission image of the cells; and Figs. 3(d) and 3(e) show the temperature changes induced by heating in the cells close to the output end of the fiber tip, caused by the absorption of laser emission by water. In this case, the maximum temperature inside cells reached up to 60 °C.

One important advantage of this method is that it can be easily adapted to an existing confocal, near-field, or other imaging system using various fluorescent labels. This method can find a wide field of applications, ranging from polymer processing to various biological studies. Temperature profiles of organelles or compartments of live cell cultures during various treatments using organelle specific or other site specific stains, and also using nanoparticles containing the dye and surface functionalized with site specific carriers for targeting.[11,18]

This work was supported by the Directorate of Chemistry and Life Sciences of the Air Force Office of Scientific Research. The authors would like to thank Dr. Tymish Ogulchansky, Dr. Yudhistir Sahoo, and Dr. Indrajit Roy for discussions and for providing nanoparticle samples. They also acknowledge Lisa Vathy and H. Jayakumar for technical assistance with samples. The authors also thank Professor Stanley Bruckenstein for helpful discussions.

[1]T. H. Gfroerer, M. D. Sturge, K. Kash, J. A. Yater, A. S. Plaut, P. S. D. Lin, J. P. Florez, L. T. Harbison, S. R. Das, and L. Lebrun, *Annual Meeting of The American Physical Society*, St. Louis, 20–24 March 1996.
[2]Z. A. Zachariasse, G. Duveneck, and R. Busse, J. Am. Chem. Soc. **106**, 1045 (1984).
[3]R. O. Luotfy and B. A. Arnold, J. Phys. Chem. **86**, 4205 (1982).
[4]A. J. Bur, M. G. Vangel, and S. Roth, Appl. Spectrosc. **56**, 174 (2002).
[5]M. L. Bhaumik, J. Chem. Phys. **40**, 3711 (1964).
[6]K. B. Migler and A. J. Bur, Polym. Eng. Sci. **38**, 213 (1998).
[7]B. I. Stepanov and V. P. Gribkovskii, *Theory of Luminescence* (Iliffe Books, London, 1968), p. 314.
[8]M. S. Chang, S. S. Elliott, T. K. Gustafson, C. Hu, and R. K. Jain, IEEE J. Quantum Electron. **8**, 527 (1972).
[9]J. L. Clark and G. Rumbles, Phys. Rev. Lett. **76**, 2037 (1996).
[10]J. L. Clark, P. F. Miller, and G. Rumbles, J. Phys. Chem. A **102**, 4428 (1998).
[11]I. Roy, T. Y. Ohulchanskyy, H. E. Pudavar, E. J. Bergey, A. R. Oseroff, J. Morgan, T. J. Dougherty, and P. N. Prasad, J. Am. Chem. Soc. **125**, 7860 (2003).
[12]R. Y. Tsien, Methods Cell Biol. **30**, 127 (1989).
[13]L. M. Loew, Methods Cell Biol. **38**, 195 (1993).
[14]A. H. Cornell-Bell, S. M. Finkbeiner, M. S. Cooper, and S. J. Smith, Science **247**, 470 (1990).
[15]B. W. Pogue, R. D. Braun, J. L. Lanzen, C. Erickson, and M. W. Dewhirst, Photochem. Photobiol. **74**, 700 (2001).
[16]B. J. F. Wong, J. P. Mark, R. Dickinson, J. Neev, and L. O. Svaasand, IEEE J. Sel. Top. Quantum Electron. **3**, 951 (1996).
[17]J. J. Eckburg, J. C. Chato, K. J. Liu, M. W. Grinstaff, H. M. Swartz, K. S. Suslick, and F. P. Auteri, J. Biomech. Eng. **116**, 193 (1996).
[18]L. Levy, Y. Sahoo, K. S. Kim, E. J. Bergey, and P. N. Prasad, Chem. Mater. **14** 3715 (2002).